First published in:

Symbols used

C_{EAQ}	[mol/L]	concentration of EAQ
C^0_{EAQ}	[mol/L]	initial concentration of EAQ
C_{EAHQ}	[mol/L]	concentration of EAHQ
EAQ	[–]	2-ethyl-9,10-anthraquinone
$EAHQ$	[–]	2-ethyl-9,10-anthrahydroquinone
f_e	[–]	catalyst wetting fraction
L_A	[mL/min]	time-average liquid flow rate
p	[kPa]	pressure
S	[–]	selectivity
$S(ss)$	[–]	selectivity for steady-state operation
T	[K]	temperature
u_G	[mm/s]	superficial gas velocity
u_L	[mm/s]	superficial liquid velocity
X	[–]	conversion
$X(ss)$	[–]	conversion for steady-state operation

Greek symbols

τ	[s]	cycle period
σ	[–]	cycle split
γ	[–]	reactant limitation criterion ($= D_{EAQ}C_{EAQ}/D_{H2}C_{H2}$)

References

[1] J. G. Boelhouwer, H. W. Piepers, B. A. H. Drinkenburg, *Chem. Eng. Technol.* **2002**, *25*, 647.
[2] P. L. Silveston, J. Hanika, *Chem. Eng. Sci.* **2002**, *57*, 3373.
[3] P. M. Haure, R. R. Hudgins, P. L. Silveston, *AIChE J.* **1989**, *35*, 1437.
[4] J. Metzinger, A. Kuehter, P. L. Silveston, S. K. Gangwal, *Chem. Eng. Sci.* **1994**, *49*, 4533.
[5] J. K. Lee, R. R. Hudgins, P. L. Silveston, *Chem. Eng. Sci.* **1995**, *50*, 2523.
[6] R. Lange et al., *Chem. Eng. Sci.* **1994**, *49*, 5615.
[7] R. Lange, R. Gutsche, J. Hanika, *Chem. Eng. Sci.* **1999**, *54*, 2569.
[8] A. T. Castellari, P. M. Haure, *AIChE J.* **1995**, *41*, 1593.
[9] L. Gabarain et al., *AIChE J.* **1997**, *43*, 166.
[10] M. Banchero, L. Manna, S. Sicardi, A. Ferri, Chem. Eng. Sci. **2004**, *59*, 4149.
[11] M. R. Khadilkar, M. H. Al-Dahhan, M. P. Dudukovic, *Chem. Eng. Sci.* **1999**, *54*, 2585.
[12] F. Turco et al., *Chem. Eng. Sci.* **2001**, *56*, 1429.
[13] B. A. Wilhite, X. Huang, M. J. McCready, A. Varma, *Ind. Eng. Chem. Res.* **2003**, *42*, 2139.
[14] D. A. Stradiotto, R. R. Hudgins, P. L. Silveston, *Chem. Eng. Sci.* **1999**, *54*, 2561.
[15] V. Tukac, J. Hanika, V. Chyba, *Catal. Today* **2003**, *79–80*, 427.
[16] G. Goor, W. Kunhel, *Ullmann's Encyclopedia of Industrial Chemistry*, VCH-Verlagsgesellschaft, Weinheim **1989**, A13, 443.
[17] J. Petr, L. Kurc, Z. Belohlav, L. Cervený, *Chem. Eng. Proc.* **2004**, *43*, 887.
[18] D. T. Burns, R. K. Harle, J. W. Ogleby, *Anal. Chimica Acta* **1978**, *100*, 563.
[19] A. A. El-Hisnawi, *Ph.D. Thesis*, Washington Univ., St. Louis, Missouri, **1981**.

Distinction between Electrostatic and Electroviscous Effects on the Permeability of Colloidal Packed Beds

By *Hermann Nirschl* and *Bastian Schäfer**

Electrostatic and electroviscous effects can significantly decrease the permeability of packed beds which consist of colloidal particles. This results in poor filterability of colloidal suspensions. Electrostatic effects refer to the dependency of the structure of the packed bed on the particles' tendency to agglomerate or disagglomerate. This tendency is influenced by the particle charge, and thus the pH and the ionic strength of the suspension. Electroviscous effects relate to the increased flow resistance of the pores due to a streaming potential being established when the electrochemical double layer of the particles is sheared off. It is difficult to distinguish electrostatic and electroviscous effects because they are interrelated. The comparison of permeability measurements of both TiO_2 and Al_2O_3 with a classical permeability model demonstrates the influence of the two different effects on permeability.

1 Introduction

In a packed bed, single colloidal particles with a medium diameter of the primary particles below 1 μm are randomly and densely distributed between two membranes while liquid flows through the porous structure. The understanding of the influences on the permeability of packed beds is important for many processes in the chemical, process, and biotechnological industries where particles are used, e.g., as a carrier for immobilized materials (catalysts, enzymes, etc.). Reactants in the liquid will interact with immobilized material on the particles. From an industrial point of view, colloidal particles have the advantage of a larger specific surface for transfer and reaction than macroscale particles. However, they cause a high flow resistance even at low volumetric flow rates in a thin layer. The results are also significant for the design of ultra- and nano-filtration processes for the separation of very fine particles in the nanometer range.

While liquid flow through a macroscopic packed bed has been very well described, many aspects of the flow through colloidal packed beds are not understood. The unsolved questions arise from the huge specific surface area of the particles, which is caused by the small particle size. Ions or other specific molecules adsorb or dissolve on the surface and produce a particle charge with an electrochemical dou-

[*] Dipl.-Ing. B. Schäfer (author to whom correspondence should be addressed, bastian.schaefer@mvm.uka.de), Prof. Dr.-Ing. H. Nirschl, Institute of Mechanical Process Engineering and Mechanics, Universität Karlsruhe (TH), Straße am Forum 8, D-76131 Karlsruhe, Germany.

  DOI: 10.1002/ceat.200500079

ble layer. This accumulation of charge influences both the structure of the packed bed and the fluid flow through the pores.

2 Classical Permeability Models

When a fluid is forced to penetrate through a porous media, the volumetric flow rate per unit area q can be calculated with D'Arcy's law [1][1]. In a generalized form, the volumetric flow rate $\frac{dV}{dt}$ per cross sectional area A can be written as a function of the pressure drop Δp, the dynamic viscosity η, and the flow resistance R:

$$q = \frac{dV}{A \cdot dt} = \frac{\Delta p}{\eta \cdot R} \tag{1}$$

The permeability K is the height of the packed bed h related to the flow resistance R [2]:

$$K = \frac{h}{R} \tag{2}$$

Different models have been proposed for the calculation of the permeability of porous media. The well established model of Carman and Kozeny [3] is based on the assumption of a Hagen-Poiseuille flow through mono-sized capillaries. Analytic transformations result in the permeability K as a function of the porosity ε and the surface-volume equivalent particle diameter x_{SV}:

$$K = \frac{1}{180} \cdot \frac{\varepsilon^3}{(1-\varepsilon)^2} \cdot x_{SV}^2 \tag{3}$$

Another popular model for the permeability of porous systems was developed by Rumpf and Gupte [4]. They found the following empirical equation:

$$K = \frac{1}{5{,}6} \cdot \varepsilon^{5,5} \cdot x_{SV}^2 \tag{4}$$

The porosity can be calculated from the mass of solid matter in the packed bed m_S, the density of the solid ρ_S, and the height h of the packed bed:

$$\varepsilon = \frac{A \cdot h - \frac{m_S}{\rho_S}}{A \cdot h} \tag{5}$$

These equations apply to macroscale packed beds. However, for the investigation of colloidal packed beds with nanoscale pores and huge specific surface areas, electrostatic and electroviscous effects have a significant influence on the permeation. It is rather evident that the equations are not able to describe the relations between the main physical quantities for the nanoscale.

1) List of symbols at the end of the paper.

3 The Electrochemical Double Layer and Zeta Potential

The surfaces of particles in water have a material specific charge which influences the distribution of ions in their vicinity. A negatively charged particle is surrounded by the inner Stern layer, a monolayer of anions, the so called co-ions, which are adsorbed due to van der Waals forces. The van der Waals forces only act on dehydrated anions because cations have a high resistance to dehydration and their radius is just too large for the short range van der Waals forces to be effective. The inner Stern layer is surrounded by a monolayer of cations, the outer Stern layer. These cations, the counter ions, are bonded by electrostatic forces. The surface charge of the particle is not fully compensated in the Stern layer, and the resulting potential at the outside of the outer Stern layer is called the Stern potential. The outer Stern layer is surrounded by a diffuse 'ion cloud'. The ion distribution in the diffuse layer is governed by the electrostatic attraction, which decreases with the distance from the surface. Thus, the ion concentration decreases and an exponential distribution results which depends on the pH value and the ionic strength of the suspension [5].

The Stern potential is not accessible by measurements. A better approach to characterize the surface charge is the zeta potential. When the particle is moved relative to the electrolytic solution, the diffuse layer is partly sheared off. The electric potential between the shear plane and the surrounding water is called zeta potential. The zeta potential is the driving force for electrokinetic effects, and can thus be calculated from measured values.

The zeta potential is positive at a low pH value. An increasing pH value leads to a decrease in the concentration of H_3O^+ ions and a lower particle charge. The zeta potential reaches zero at a material specific pH value, the isoelectric point (IEP) and becomes negative beyond the IEP. Since solute ions block the electrochemical potential, the zeta potential will have low values for suspensions with a high concentration of ions.

4 Electrostatic, Electrokinetic and Electroviscous Effects

According to the DLVO theory, the stability of colloidal suspensions is determined by the equilibrium of the repulsive and attractive forces, with electrostatic repulsion, van der Waals attraction, and Born's repulsion being the most important contributions.

Particles with low surface charge agglomerate due to attractive van der Waals forces. Packed beds formed by filtration of an agglomerated suspension have a loose structure and a high porosity. The pore size distribution is very inhomogeneous and permeating water will mainly flow through the big pores between the agglomerates, while the inner pores of the agglomerates are hardly affected. In contrast,

suspensions with high surface charging are stabilized by electrostatic repulsion. Packed beds formed by filtration of a stable dispersion have a compact structure with a low porosity. The pore size distribution is homogenous and a high flow resistance results.

Under application of an electrostatic potential or a pressure difference, the ions in the diffuse layer are sheared apart from the particle surfaces. The classical theory of electrokinetics describes two electrokinetic effects, which influence the flow through colloidal packed beds [6]:

– **Electroosmosis** is the flow of a liquid in a confined and charged structure caused by the application of an electric potential. The ions in the diffuse layer are accelerated by the electric field. The water molecules adjacent to the ions are dragged by viscous forces, and a volumetric flow results.
– The **streaming potential** can be measured when a liquid is driven through a confined and charged structure. The moveable ions in the diffuse layer are sheared off by drag forces. A charge transport takes place and an electric potential is built up.

The streaming potential leads to an electroosmotic flow against the direction of the pressure driven flow. This so called **electroviscous effect** retards the pressure driven flow and leads to a steady state of the streaming potential.

The influence of the electrostatic effect on the permeability of filter cakes has been investigated [7, 8]. The electroviscous effect has been investigated for flow in microchannels [9] and in colloidal suspensions [10]. We do not know of any model describing how the combination of electrostatic and electroviscous effects influences the permeability of colloidal packed beds.

5 Materials and Experimental Setup

The experiments where carried out in a Compression-Permeability cell (CP cell) (see Fig. 1). In the CP cell the packed bed is formed by the filtration of a suspension of nanoscalic particles between two membranes inside a cylindrical device. The upper membrane of the packed bed is compressed to defined pressures by a plunger and the filtrate drains through the lower membrane onto a scale. Nylon membranes with a nominal pore diameter of 0.2 μm (Pall, USA) were chosen as the filter media. Bridge formation on the membrane retards the small particles from passing the relatively large membrane pores. The thickness of the particle bed is in the range of some millimeters.

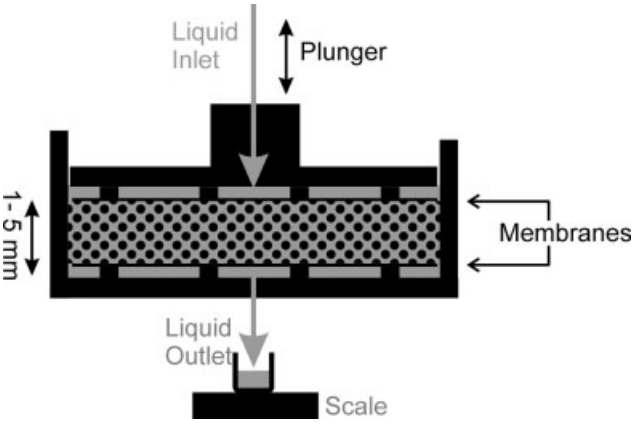

Figure 1. Compression-permeability cell.

After a steady state of compression is reached, this is when the filtrate flux abates, a valve at the permeate inlet is opened. Pressurized de-ionized water starts to flow through the plunger into the chamber above the upper membrane, permeates the packed bed, and leaves the CP-cell onto the scale.

Titanium dioxide particles (Aeroxide TiO_2, P25, Degussa, Germany) with a purity of 99.5 %, a primary particle size of 21 nm, and a specific surface area (BET) of 50 ± 15 m^2/g [11] were used. The suspension was prepared by mixing the particles and an aqueous solution of nitric acid or caustic potash in order to vary the pH value, so that different levels of zeta potential were obtained. The suspension is dispersed in an ultrasonic bath and evacuated at a pressure of 5 kPa. Fig. 2 shows the agglomerates in a suspension with a pH value of 11.5. Since the particles are connected by strong sinter bridges, the particles are not fully dispersed but form agglomerates of heterogeneous size. The dark holes in Fig. 2 represent the pores of the REM grid.

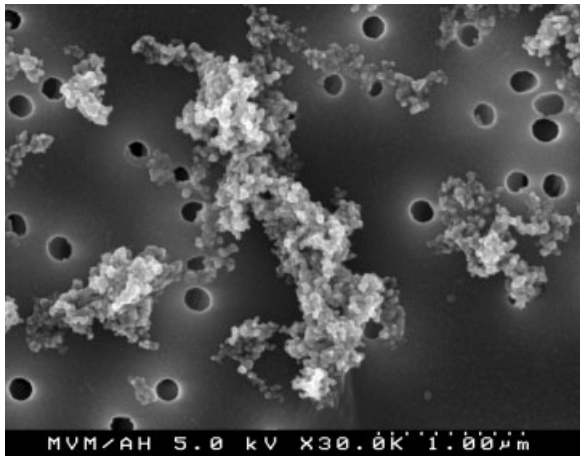

Figure 2. REM picture of TiO_2 agglomerates.

The measurements with Al_2O_3 [12] were made with particles MR70 (Martinswerke Frechen, Germany) with an average primary particle size of 263 nm and a specific surface area of 8 m^2/g. The pH value was varied with hydrochloric acid and sodium hydroxide. The Al_2O_3 agglomerates consist of only a few irregularly shaped particles.

6 Results and Discussion

The influence of the zeta potential on the permeability and on the porosity of packed beds consisting of Al_2O_3 and

TiO_2 is shown in Fig. 3 and Fig. 5 at different pressure levels. The packed beds show compressible behavior, i.e., porosity and permeability strongly depend on the applied pressure which is transmitted by the plunger of the CP-cell. The influence of the pressure is more significant at the IEP, where the zeta potential is zero and the particles are thus agglomerated. Compression leads to a reduction of the porosity and permeability with a shrinking of the large pores between the agglomerates. The agglomerates are probably not disrupted, they are just deformed.

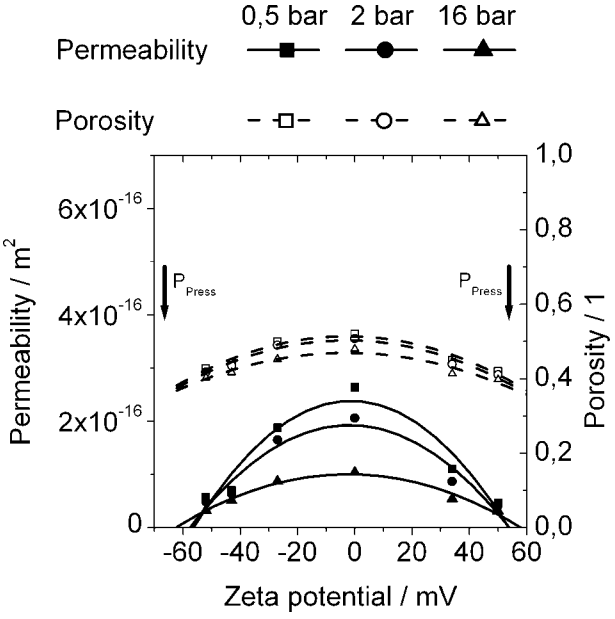

Figure 3. Permeability and porosity of Al_2O_3. The curves represent second order polynomial fits.

A strong particle charge, with either positive or negative algebraic sign, prevents agglomeration and leads to a densely packed structure. The dense structure permits less compression than a loose structure. Furthermore, the repulsion of the particles limits their approach to each other. Therefore, a colloidal packed bed permits less deformation when the surface charge is higher. We can conclude that both higher particle charging and higher compression will cause a more homogeneous structure with a minimum porosity.

Porosity and permeability of the Al_2O_3 packed bed strongly depend on the zeta potential, as shown in Fig. 3. They are significantly higher in the vicinity of the IEP than in the region of high surface charge. These relations are symmetric with respect to the IEP as the observed electrostatic and electroviscous effects only depend on the absolute value of the particle charge. The strong dependency of the porosity on the zeta potential can be explained by the agglomeration of the small Al_2O_3 aggregates in the region of the IEP, as already discussed in section 4.

Fig. 4 shows a comparison of the measured permeability of the packed beds with the permeability calculated with the empirical Rumpf-Gupte model [4]. The calculated permeabilities of the Al_2O_3 packed bed show, in principle, the same dependency on the zeta potential as the measured values. The differences for the single values could arise from the non-spherical particle shapes of the measured material. This influence is not taken in to account in the empirical model. However, in nanoscalic dimensions the geometry effect should be minor compared to the effects arising from the big surfaces. We presume that the dependence of the permeability on the surface charge can be assigned to structural changes of the packed bed.

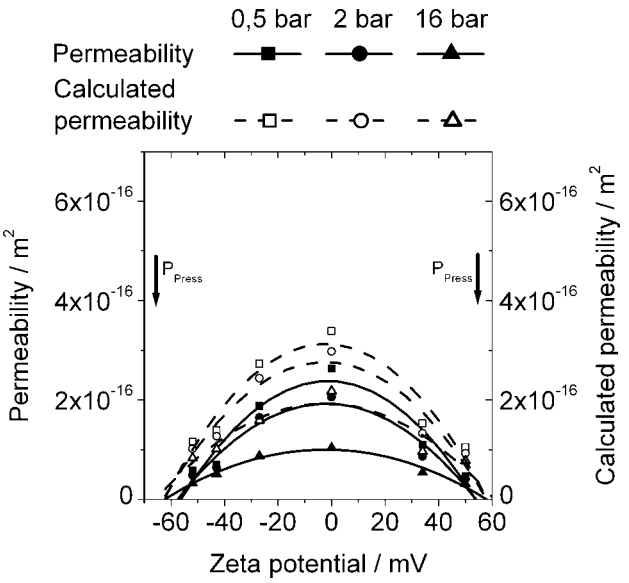

Figure 4. Comparison of the measured permeability with the permeability calculated with the Rumpf-Gupte model for Al_2O_3. The curves represent second order polynomial fits.

In principle the same correlations can be observed for TiO_2. The permeability of the TiO_2 packed bed is higher for pH values close to the IEP than for pH values corresponding to high surface charge. The deviation of the maximum permeability from the IEP presumably arises from measuring errors and problems of numerical adjustment. A difference to the Al_2O_3 particles is visible for the porosities. The small influence of the pH value on the porosity can be explained by the strong sinter bridges in the TiO_2 agglomerates, which can not be affected by high particle charging.

The deviation of the calculated permeability from the measurements is significantly stronger for TiO_2 than for Al_2O_3 (see Figs. 5 and 6). The calculated permeability hardly changes with pH value. The strong dependency of the measured permeability thus can not be explained by structural changes. The changes must be a result of electroviscous effects. The higher importance of the electroviscous effect for TiO_2 packed beds than for Al_2O_3 packed beds can be explained by the much higher specific surface area of the TiO_2 particles, which allows a higher number of ions to bond to the surface. The TiO_2 packed beds were compressed to different pressure levels than the Al_2O_3 packed beds because of construction limitations.

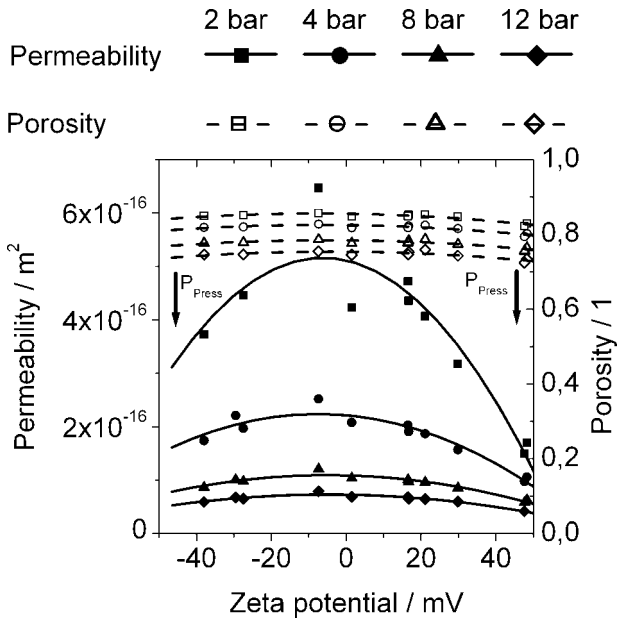

Figure 5. Permeability and porosity of TiO_2. The curves represent second order polynomial fits.

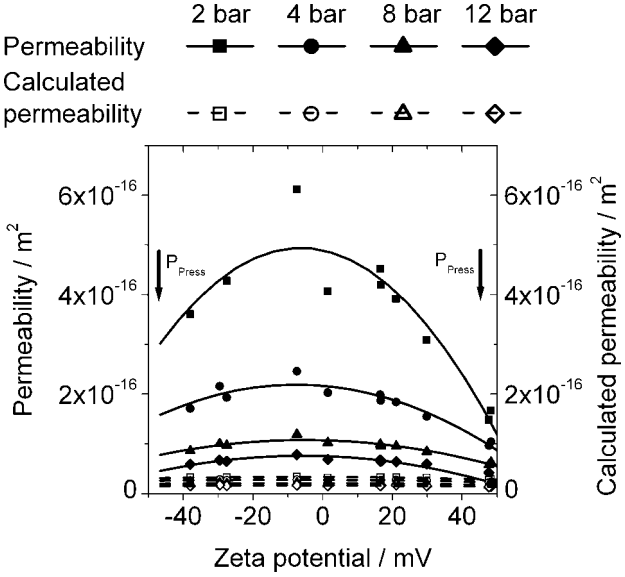

Figure 6. Comparison of the measured permeability with the permeability calculated with the Rumpf-Gupte model for TiO_2. The curves represent second order polynomial fits.

7 Summary

The permeability of colloidal packed beds is dominated by electrostatic and electroviscous effects, which originate from the surface charging of the particles and, thus, the pH value of the suspension. The distinction between electrostatic and electroviscous effects on the permeability of packed beds is difficult since they always occur together. While the electrostatic effect denotes the impact of particle charge on the structure and thus the permeability of the packed bed, the electroviscous effect is the influence of ion motion on the permeability of a fine particulate system.

The permeability of packed beds of Al_2O_3 particles and of TiO_2 was measured for different pH values and, therefore, zeta potentials of the suspension. A comparison with the classical permeability model from Rumpf and Gupte shows that for Al_2O_3 the permeability variation can be explained by the electrostatic effect to a large extent. For TiO_2 the permeability variation can not be explained by the electrostatic effect since the porosity does not depend on the pH value. Therefore, the permeability variation must result from the electroviscous effect.

Acknowledgments

The authors wish to thank the Deutsche Forschungsgemeinschaft (Priority Program 1164) for financial support.

Received: March 7, 2005 [CET 0079]

Symbols used

A	cross sectional area
h	height of the packed bed
K	permeability
m_S	mass of solid matter in the packed bed
q	volumetric flow rate per unit area
R	flow resistance
V	volume
x_{SV}	surface-volume equivalent particle diameter
Δp	pressure drop
ε	porosity
η	dynamic viscosity
ρ_S	density of the solid

References

[1] H. D'Arcy, *Les Fontaines Publiques de la Ville de Dijon, Libraire des Corps Impériaux des Ponts et Chaussées et des Mines*, Dalmont, Paris **1856**.
[2] J. A. Sorrentino, *Ph.D. Thesis*, Universität Karlsruhe (TH) **2003**.
[3] P. C. Carman, *Trans. Inst. Chem. Eng., London,* **1937**, *15*, 150.
[4] H. Rumpf, A. R. Gupte, Translation into English from *Chem. Ing. Tech.* **1971**, *43 (6)*, 367.
[5] J. Lyklema, *Fundamentals of Interface and Colloid Science*, Academic Press, London **1992**.
[6] R. J. Hunter, *Zeta-Potential in Colloid Science*, Academic Press, London **1981**.
[7] S. A. Lee, A. G. Fane, R. Amal, T. D. Waite, *Separ. Sci. Technol.* **2003**, *38 (4)*, 869.
[8] L. F. Fu, B. A. Dempsey, *J. Membrane Sci.* **1998**, *149*, 221.
[9] C. L. Ren, D. Q. Li, *J. Colloid Interf. Sci.* **2004**, *274*, 319.
[10] F. J. Rubio-Hernandez, F. Carrique, E. Ruiz-Reina, *Adv. Colloid Interf.* **2004**, *107*, 51.
[11] Degussa, *Product Information AEROXIDE® TiO_2 P 25*, **2004**. Available online: https://www1.sivento.com.
[12] J. Heuser, *Ph.D. Thesis*, Universität Karlsruhe (TH) **2003**.

